NANO: Brief Reports and Reviews
Vol. 11, No. 4 (2016) 1650043 (6 pages)

DOI: 10.1142/S1793292016500430

World Scientific
www.worldscientific.com

Vibrational Analysis of a Single-Layered Nanoporous Graphene Membrane

Haw-Long Lee and Win-Jin Chang*
Department of Mechanical Engineering
Kun Shan University, Tainan 71003, Taiwan
**changwj@mail.ksu.edu.tw*

Received 4 November 2015
Accepted 8 December 2015
Published 21 January 2016

In this study, we use the atomic-scale finite element method to investigate the vibrational behavior of the armchair- and zigzag-structured nanoporous graphene layers with simply supported-free-simply supported-free (SFSF) and clamped-free-free-free (CFFF) boundary conditions. The fundamental frequencies computed for the graphene layers without pores are compared with the results of previous studies. We observe very good correspondence of our results with that of the other studies in all the considered cases. For the armchair- and zigzag-structured nanoporous graphenes with SFSF and CFFF boundary conditions, the frequencies decrease with increasing porosity. When the positions of the pores are symmetric with respect to the center of the graphene, the frequency of the zigzag nanoporous graphene is higher than that of the armchair one. To the best of our knowledge, this is first study investigating the relation between the vibrational behavior and porosity of nanoporous graphene layers, which is essential for tuning the material/structural design and exploring new applications for nanoporous graphenes.

Keywords: Graphene; nanoporous; natural frequency.
PACS Nos.: 43.40.+s, 61.48.Gh, 62.25.Jk.

1. Introduction

Graphene has recently attracted significant research interest because of its excellent physical and chemical properties.[1–5] Owing to these lucrative properties, graphene is currently studied for its potential applications in nanobiological devices and nanomechanical systems. In addition, nanoporous graphene has also been widely investigated for its high selectivity and unique permeability.[6–8] It can be applied in various fields such as atmospheric nanofilters,[9] gas separation,[10] nanopore biodiffusion,[11] detection of environmental hazards,[12] molecular motors,[13] molecular sieves,[14–16] and protein and DNA analysis.[17–19]

In 2009, Bieri *et al.*,[20] for the first time, succeeded in synthesizing a well-defined nanoporous graphene. Since then, a number of other related studies have appeared in the literature. For example, Cohen-Tanugi and Grossman[21] investigated nanometer-scale pores in single-layer freestanding graphene and examined the desalination dynamics change with pore size, pore chemistry and applied hydrostatic pressure using molecular dynamics simulations. They found that the water permeability of this material is

several orders of magnitude higher than that of the conventional reverse osmosis membranes, and that nanoporous graphene may play a valuable role in water purification. Recently, Ito *et al.*[22] developed a nanoporous Ni-based chemical vapor deposition technique for the growth of high-quality nanoporous graphene. They found that the transport properties of the nanoporous graphene showed a semiconducting behavior and strong pore size dependence, coupled with unique angular independence. Liu and Chen[23] performed molecular dynamics simulations to study the mechanical properties of nanoporous graphene with different sizes, shapes, and densities of nanopores, and found that the strength decreased as the size and porosity of the nanopore increased.

Since performing experiments on nanoscale materials such as graphenes with pores are extremely challenging, theoretical methods, including atomistic simulations[23] and continuum mechanics modeling, are often adopted. However, molecular dynamic simulations are computational-time intensive approaches. Moreover, the case for nanoporous graphenes cannot be easily solved by using analytical and numerical methods such as the classical Rayleigh–Ritz method. Therefore, we used the commercial finite element program, ANSYS, for this study. In this study, the atomic-scale finite element model is used to investigate the vibrational behavior of nanoporous graphene. The graphene is considered to have a frame-like structure. Their bonds are considered as beam elements and all the joints host the carbon atoms. Based on this model, the effects of pore location and porosity on the vibrational frequency of graphene with different boundary conditions are analyzed. To our knowledge, this is the first report on the vibrational behavior of nanoporous graphene.

2. Atomic Finite Element Analysis

A single layer of graphene in the ANSYS package is simulated as a frame-like structure with beam members. The bonds between the carbon atoms are described as connecting load-carrying members, while the carbon atoms are considered as joints of the connecting members. The configurations of different nanoporous square-outline graphene layers with length L, having an average diameter of about 1.1 nm for each pore, are shown in Fig. 1. The origin is the lower-left corner of the square-outline graphene. The symbol x represents the armchair direction and y represents the zigzag direction r_x and r_y represent the distance from the origin to the center of the single pore in the x- and y-directions, respectively. All the pores are arranged in a symmetric fashion with respect to the center of the graphene.

In this paper, the commercial finite element program, ANSYS, is used to analyze the vibration behavior of the nanoporous graphene. The model used in the analysis is the same with the previous study.[24] The deformation of the single-layer graphene as a space-frame structure can be estimated by formulating a relationship between structural mechanics and molecular mechanics.[25] From the perspective of molecular mechanics, the total potential energy due to bonded interactions for the single layer graphene can be expressed by the following equation:

$$U_{\text{tot}} = \sum U_r + \sum U_\theta + \sum U_\tau, \tag{1}$$

where U_r, U_θ and U_τ are the energies associated with bond stretching, bending and torsion, respectively.

In addition, the total strain energy of a beam member from a structural mechanics viewpoint is given by the following equation:

$$U_{\text{tot}} = \sum U_A + \sum U_B + \sum U_T, \tag{2}$$

where U_A, U_B and U_T are the strain energies due to axial tension, bending and torsion, respectively.

In order to obtain a relationship between the force constants in molecular mechanics and the beam element stiffness values in structural mechanics, an energy equivalence concept[25] is employed in Eqs. (1) and (2). The following relationship can be established based on the energy equivalence[25]:

$$\frac{EA}{\ell} = k_r, \quad \frac{EI}{\ell} = k_\theta, \quad \frac{GJ}{\ell} = k_\tau, \tag{3}$$

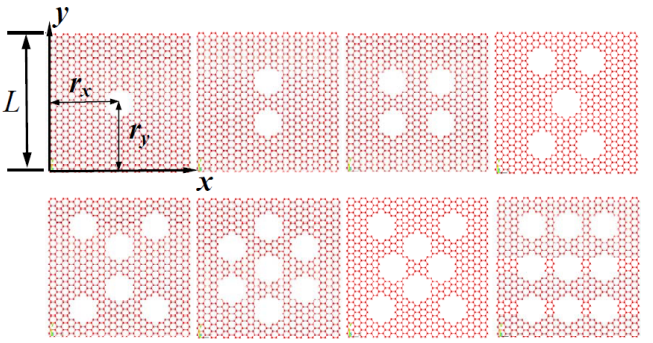

Fig. 1. The configurations of different nanoporous square graphene with length L. x is the armchair direction and y is the zigzag direction.

where A, I and J are the area, bending moment of inertia and polar moment of inertia of the graphene cross-section, respectively. E and G denote the Young's modulus and shear modulus of the graphene, respectively. ℓ is the covalent bond length of the carbon atoms in the hexagonal lattice. k_r, k_θ and k_r are the force constants in molecular mechanics and they represent the capabilities of tensile resistance, flexural rigidity and torsional stiffness, respectively.

Using Eq. (3), the following parameters can be estimated from Ref. 24, where d is the covalent bond diameter.

$$d = 4\sqrt{\frac{K_\theta}{K_r}}, \quad E = \frac{\ell K_r^2}{4\pi K_\theta}, \quad G = \frac{\ell K_r K_\theta^2}{8\pi K_r^2} \qquad (4)$$

3. Results and Discussion

To verify the accuracy of our ANSYS model for calculating the vibration frequency of graphene, we compare the present result with the previous study, where the following parameters were used[24]: $\ell = 0.142\,\text{nm}$, $h = 0.34\,\text{nm}$, $L = 5\,\text{nm}$, $K_r = 6.52 \times 10^{-7}\,\text{N/nm}$, $K_\theta = 8.76 \times 10^{-10}\,\text{N·nm/rad}^2$, $K_\tau = 2.78 \times 10^{-10}\,\text{N·nm/rad}^2$, $d = 1.466\text{Å}$, $E = 5.488 \times 10^{-8}\,\text{N/Å}^2$, $G = 8.701 \times 10^{-9}\,\text{N/Å}^2$. Both simply supported-free- simply supported-free (SFSF) and clamped-free-free-free (CFFF) boundary conditions are considered in the analysis. For an armchair graphene of size 5 nm without pores, the frequencies obtained from the present study are 44.5 GHz and 15.4 GHz for the cases of SFSF and CFFF, respectively. Similarly, the frequencies of the zigzag structure were computed to be 45.8 GHz and 15.9 GHz for the cases of SFSF and CFFF, respectively. These results are in very good agreement with previously reported Fig. 13(a) of Ref. 24.

The fundamental frequency of the graphene layer having a pore with SFSF boundary conditions at different pore locations for the cases $r_y/L = 1/2$ and $r_x/L = 1/2$ are shown in Figs. 2(a) and 2(b). It can be observed that the frequencies of the armchair and zigzag graphene layers, with pores as shown in Fig. 2(a), are symmetric with respect to the $r_x/L = 1/2$ line and the others, as shown in Fig. 2(b), are also symmetric with respect to the $r_y/L = 1/2$ line due to the symmetric boundary conditions and geometric structure. The frequencies of the armchair and zigzag graphenes having pores with SFSF boundary conditions are always lower than that of the case with no pores (i.e., 44.5 GHz for armchair and 45.8 GHz for zigzag). For the armchair graphene, as shown in Fig. 2(a), the frequency is the minimum for the pore location at $r_x/L = 0.5$. This is because the pore at the center results in a graphene with a lower stiffness than that at other locations along the x-direction. This also indicates that a higher frequency is obtained when the pore is further away from the center along the x-direction. However, the situation is different for zigzag graphene. The effect of pores on the frequency of the zigzag graphene is minimal owing to the constraint imposed on the movement direction of the pore. The

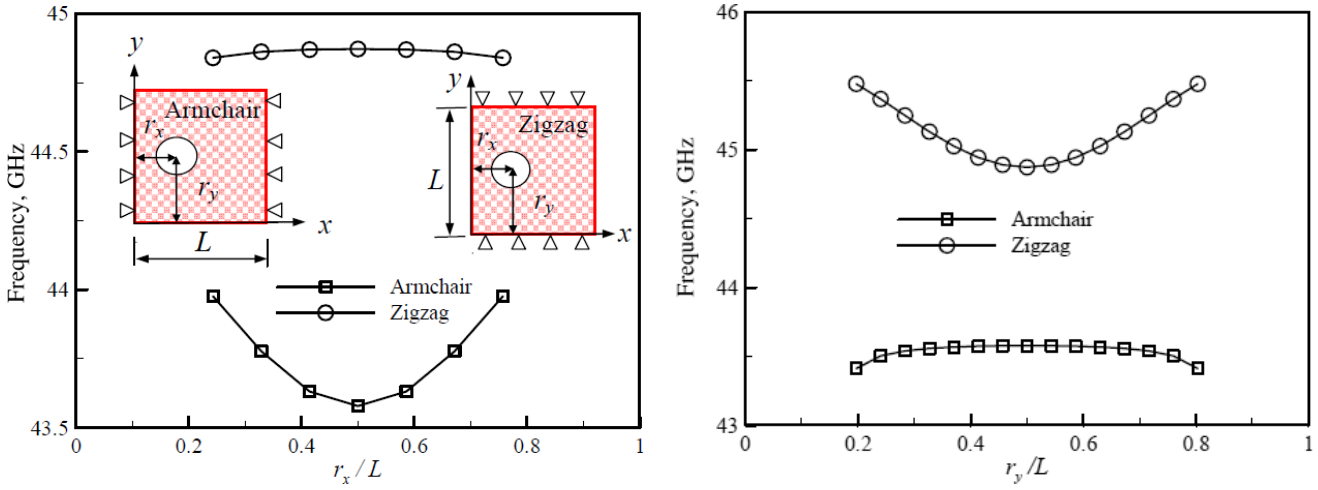

Fig. 2. The fundamental frequency of the graphene having a hole with SFSF boundary conditions at different hole locations for (a) $r_y/L = 1/2$ and (b) $r_x/L = 1/2$.

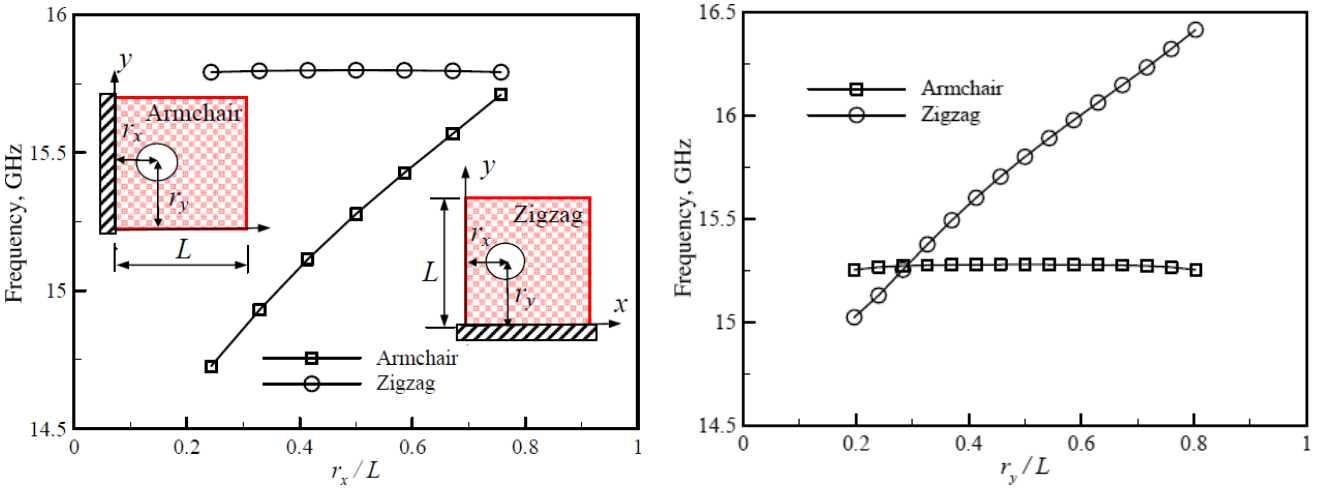

Fig. 3. The fundamental frequency of the graphene having a hole with CFFF boundary conditions at different hole locations for (a) $r_y/L = 1/2$ and (b) $r_x/L = 1/2$.

maximum frequency is obtained at $r_x/L = 0.5$. The reason is that the effect of stiffness loss on the frequency can be negligible when the movement direction of the pore is parallel to the constraint edges. However, the effect of mass loss due to the pore at the center of the graphene is slightly greater than that at other locations along the x-direction.

In contrast to Figs. 2(a), the trend is reversed for the frequencies of the armchair and zigzag graphenes with a pore along the y-direction, as shown in Fig. 2(b). For both Figs. 2(a) and 2(b), the frequency of the zigzag graphene having a pore with SFSF boundary conditions is higher than that of the armchair one. The trend remains the same for graphene without a pore under the same conditions.[24]

The fundamental frequencies of the graphene layer having a pore with CFFF boundary conditions at different pore locations for the cases of $r_y/L = 1/2$ and $r_x/L = 1/2$ are represented in Figs. 3(a) and 3(b), respectively. In contrast to the frequency of the graphene layer with SFSF boundary conditions, as shown in Fig. 2, the frequency of graphene having a pore with CFFF boundary conditions is lower. Moreover, the frequency of the graphene layer with CFFF boundary conditions is not symmetric unlike that of SFSF graphene. It can be seen from Fig. 3(a) that the effect of pores on the frequency of the armchair graphene is significant. The frequency increases with an increase of the position of the pore away from the clamped edge, because the equivalent mass loss effect induced by the pore increases as the distance of the pore away from the fixed end is increased. However, the effect of pores on the zigzag structure can be negligible due to the constraint imposed by graphene. The trend is reversed for the frequency of the armchair and zigzag graphenes, with a pore along the y-direction, as shown in Fig. 3(b).

For the case of CFFF boundary conditions, the results in Fig. 3(b) show that the chirality does not have a significant influence. A similar trend is obtained from the study by Chowdhury *et al.*,[26] who carried out the frequency analysis of zigzag and armchair single-layer graphene sheets without pores using the molecular mechanics method. The frequency values were 15.4 GHz and 15.9 GHz, as mentioned before for the perfect armchair and zigzag graphenes with CFFF boundary conditions, respectively. The frequency is independent of the pore when the pore is located at an appropriate position. This indicates that the mass loss effect on the frequency of the graphene with a pore is equivalent to the reduction of stiffness. According to the analysis, the intersection of the frequency is at about $r_x/L = r_y/L = 0.6$. For the armchair graphene, as shown in Fig. 3(a), the frequency is higher than that of the perfect graphene layer, when the pore location is farther than $r_x/L = 0.6$. The situation is reversed when the pore location is closer than $r_x/L = 0.6$. Similar phenomena can also be observed for the case of the zigzag graphene, as shown in Fig. 3(b). The critical transition position is at $r_y/L = 0.6$.

Figures 4 and 5 show the relationship between the fundamental frequency and porosity. Positivity is

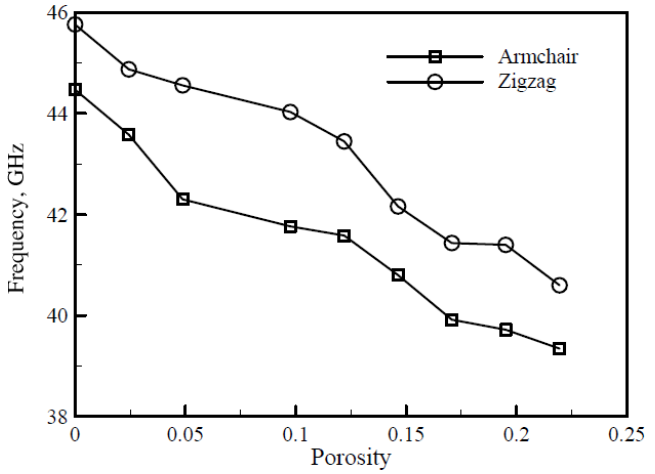

Fig. 4. The fundamental frequency of the nanoporous graphene with different porosities for SFSF boundary conditions.

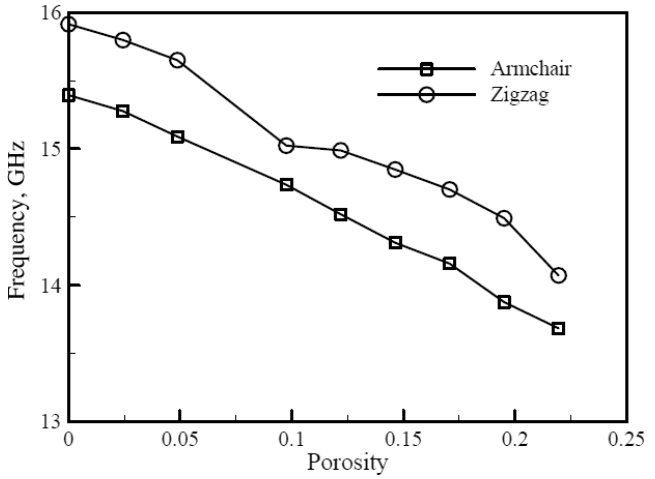

Fig. 5. The fundamental frequency of the nanoporous graphene with different porosities for CFFF boundary conditions.

defined to be the ratio between missing atoms and the total atoms of the pristine graphene of the same size.[23] The value of porosity used in the abscissa of Figs. 4 and 5 is obtained from Fig. 1. The value increases with the number of pores. Figure 4 illustrates the fundamental frequency of the nanoporous graphene with different porosities for SFSF boundary conditions. The configurations of the nanoporous graphene with different pore types are shown in Fig. 1. The frequencies of the armchair and zigzag nanoporous graphenes decrease with an increase of porosity because of the decrease in stiffness of the nanoporous graphene. In addition, the frequency of the zigzag porous graphene is higher than that of the armchair one.

Figure 5 depicts the fundamental frequency of the nanoporous graphene with different porosities for CFFF boundary conditions. Similar to the case of SFSF boundary conditions, as shown in Fig. 4, the frequencies of the armchair and zigzag nanoporous graphene layers decrease with an increase of porosity. The frequency of the zigzag porous graphene is higher than that of the armchair one.

4. Conclusions

In this study, the effects of the pore location and porosity on the vibrational behavior of the armchair and zigzag nanoporous graphene layers with SFSF and CFFF boundary conditions were analyzed using the atomic-scale finite element method. Based on the analysis, the following results were obtained:

1. The frequencies of the armchair- and zigzag-structured nanoporous graphene layers having a pore with SFSF boundary conditions were always lower than that for the layers without pores. However, the situation was different for the case of CFFF boundary conditions.
2. For the armchair graphene, the frequency was higher than that of perfect graphene when the pore location was farther than $r_x/L = 0.6$. The situation was reversed when the pore location was closer than $r_x/L = 0.6$. Similar trends were observed for the case of the zigzag graphene as well. The critical transition position for the pore was found to be at $r_y/L = 0.6$.
3. For the armchair- and zigzag-structured nanoporous graphenes with SFSF and CFFF boundary conditions, the frequencies decreased with an increase of porosity.
4. The frequencies in the zigzag porous graphene structures with SFSF and CFFF boundary conditions were higher than those observed for the armchair graphene structures.

Acknowledgment

The authors wish to thank the Ministry of Science and Technology of Taiwan for providing financial supports for this study under projects MOST 103-2221-E-168-014 and MOST 103-2221-E-168-006.

References

1. A. K. Geim and K. S. Novoselov, *Nat. Mater.* **6**, 183 (2007).
2. A. H. C. Neto, F. Guinea, N. M. R. Peres, K. S. Novoselov and A. K. Geim, *Rev. Mod. Phys.* **81**, 109 (2009).

3. S. Wang, B. Yang, S. Zhang, J. Yuan, Y. Si and H. Chen, *Chem. Phys. Chem.* **15**, 2749 (2014).
4. B. Yang, S. Wang, Y. Guo, J. Yuan, Y. Si, S. Zhang and H. Chen, *RSC Adv.* **4**, 54677 (2014).
5. S. Wang, B. Yang, J. Yuan, Y. Si and H. Chen, *Sci. Rep.* **5**, 14957 (2015).
6. K. S. Novoselov, A. K. Geim, S. V. Morozov, D. Jiang, Y. Zhang, S. V. Dubonos, I. V. Grigorieva and A. A. Firsov, *Science* **306**, 666 (2004).
7. C. N. R. Rao and A. K. Sood (eds). *Graphene: Synthesis, Properties, and Phenomena* (Wiley. com, 2013).
8. W. Yuan, J. Chen and G. Shi, *Mater. Today* **17**, 77 (2014).
9. S. Blankenburg, M. Bieri, R. Fasel, K. Mullen, C. A. Pignedoli and D. Passerone, *Small* **6**, 2266 (2010).
10. D. Jiang, V. R. Cooper and S. Dai, *Nano Lett.* **9**, 4019 (2012).
11. V. Berry, *Carbon* **62**, 1 (2013).
12. P. Xu, H. Yu and X. Li, *Chem. Commun.* **48**, 10784 (2012).
13. J. H. Lee, J. Y. Tan, C. T. Toh, S. P. Koenig, V. E. Fedorov, A. H. C. Neto and B. Ozyilmaz, *Nano Lett.* **14**, 2677 (2014).
14. S. P. Koenig, L. Wang, J. Pellegrino and J. S. Bunch, *Nat. Nanotechnol.* **7**, 728 (2012).
15. R. K. Joshi, P. Carbone, F. C. Wang, V. G. Kravets, Y. Su, I. V. Grigorieva, H. A. Wu, A. K. Geim and R. R. Nair, *Science* **343**, 752 (2014).
16. H. Chen and E. Ruckenstein, *J. Phys. Chem. Lett.* **5**, 2979 (2014).
17. E. L. Bonome, R. Lepore, D. Raimondo, F. Cecconi, A. Tramontano and M. Chinappi, *J. Phys. Chem. B* **119**, 5815 (2015).
18. G. T. Feliciano, C. Sanz-Navarro, M. D. Coutinho-Neto, P. Ordejón, R. H. Scheicher and A. R. Rocha, *Phys. Rev. Appl.* **3**, 034003 (2015).
19. H. L. McFarland, T. Ahmed, J. X. Zhu, A. V. Balatsky and J. T. Haraldsen, *J. Phys. Chem. Lett.* **6**, 2616 (2015).
20. M. Bieri, M. Treier, J. Cai, K. Aït-Mansour, P. Ruffieux, O. Gröning, P. Gröning, M. Kastler, R. Rieger, X. Feng, K. Müllen and R. Fasel, *Chem. Commun.* **45**, 6919 (2009).
21. D. Cohen-Tanugi and J. C. Grossman, *Nano Lett.* **12**, 3602 (2012).
22. Y. Ito, Y. Tanabe, H. J. Qiu, K. Sugawara, S. Heguri, N. H. Tu, K. K. Huynh, T. Fujita, T. Takahashi, K. Tanigaki and M. Chen, *Angew. Chem.* **126**, 4922 (2014).
23. Y. Liu and X. Chen, *J. Appl. Phys.* **115**, 034303 (2014).
24. S. Rouhi and R. Ansari, *Physica E* **44**, 764 (2012).
25. C. Li and T. W. Chou, *Int. J. Solids Struct.* **40**, 2487 (2003).
26. R. Chowdhury, S. Adhikari, F. Scarpa and M. I. Friswell, *J. Phys. D Appl. Phys.* **44**, 205401 (2011).